Detection of human influence on twentieth-century precipitation trends

Xuebin Zhang[1], Francis W. Zwiers[1], Gabriele C. Hegerl[2], F. Hugo Lambert[3], Nathan P. Gillett[4], Susan Solomon[5], Peter A. Stott[6] & Toru Nozawa[7]

Human influence on climate has been detected in surface air temperature[1–5], sea level pressure[6], free atmospheric temperature[7], tropopause height[8] and ocean heat content[9]. Human-induced changes have not, however, previously been detected in precipitation at the global scale[10–12], partly because changes in precipitation in different regions cancel each other out and thereby reduce the strength of the global average signal[13–19]. Models suggest that anthropogenic forcing should have caused a small increase in global mean precipitation and a latitudinal redistribution of precipitation, increasing precipitation at high latitudes, decreasing precipitation at sub-tropical latitudes[15,18,19], and possibly changing the distribution of precipitation within the tropics by shifting the position of the Intertropical Convergence Zone[20]. Here we compare observed changes in land precipitation during the twentieth century averaged over latitudinal bands with changes simulated by fourteen climate models. We show that anthropogenic forcing has had a detectable influence on observed changes in average precipitation within latitudinal bands, and that these changes cannot be explained by internal climate variability or natural forcing. We estimate that anthropogenic forcing contributed significantly to observed increases in precipitation in the Northern Hemisphere mid-latitudes, drying in the Northern Hemisphere subtropics and tropics, and moistening in the Southern Hemisphere subtropics and deep tropics. The observed changes, which are larger than estimated from model simulations, may have already had significant effects on ecosystems, agriculture and human health in regions that are sensitive to changes in precipitation, such as the Sahel.

We used monthly precipitation observations over global land areas from the most recent version of the Global Historical Climatology Network (GHCN)[21] to analyse precipitation trends in two twentieth-century periods (1925–1999 and 1950–1999), during which observational data are considered to be sufficient to describe global-scale land precipitation change. This data set has been carefully quality controlled. Previous studies of external influence on global precipitation changes[10–12] used a gridded data set[22] based on an earlier version of the GHCN that was less complete during the last few years of the twentieth century; we obtained similar results when using this original data set. We focused on the region 40° S–70° N because observational coverage elsewhere is limited.

We compared observed trends to those simulated by a large number of climate models to determine whether observed changes over the two twentieth-century periods have been caused by external influences on the climate system. The climate simulations were obtained from the multi-model data archive at PCMDI (http://www-pcmdi.llnl.gov/ipcc/about_ipcc.php) and from modelling centres directly. We considered three groups of twentieth-century simulations. One group (ANT) includes 27 simulations conducted with 8 models forced with estimates of historical anthropogenic forcing only, including greenhouse gases and sulphate aerosols. A second group (ALL) includes 50 simulations conducted with 10 models forced with estimates of both historical anthropogenic and natural external forcing, including volcanic aerosols and solar irradiance change. A third group (NAT4) includes 15 simulations conducted with 4 models forced with natural external forcing only. Slightly different configurations of historical forcing were used by different modelling centres[12]. The make-up of each group and the number of simulations used from each model is summarized in Supplementary Table 1. Four models (ECHO-G, HadCM3, MIROC, PCM) contributed simulations to all three groups; the subsets of ANT and ALL simulations from these models are referred to as ANT4 and ALL4 respectively.

We analysed trends in annual zonal mean precipitation anomalies expressed relative to 1961–90. Trends in observed and simulated precipitation were computed and compared quantitatively using the 'optimal fingerprint' method[23,24], a regression procedure that has been used in many previous detection studies[1].

Linear precipitation trends from observations and the average of multiple model simulations for 1925–1999 (Figs 1 and 2) exhibit important areas of consistency in the spatial distribution of precipitation change. Both observations and models show that precipitation increased in the Southern Hemisphere deep tropics and subtropics, decreased in the Northern Hemisphere tropics and subtropics, and increased in the Northern Hemisphere poleward of 50° N. We note an important difference, however: observations suggest a slight upward trend in zonal precipitation between about 20–40° N, while the mean ALL simulation shows a slight downward trend (Fig. 1a). Also we note that uncertainty in model-simulated trends is high: the range of trends from available simulations includes zero for all latitudinal bands, indicating that the simulated change in individual latitude bands could be explained by internal variability. However, the pattern of precipitation change across different latitudes may still allow detection. The observed latitudinal pattern of precipitation trends correlates well with the all-forcings multi-model simulated pattern (correlation 0.83 for the 75-year trend, Fig. 1a, compared to 0.69 for the ANT simulations, Fig. 1b, and 0.02 for the NAT4 simulations, Fig. 1c). We obtained similar results from the 50-year trends (Fig. 1d–f). Differences in zonal precipitation trends between different models are greater than those between individual ensemble members from the same model, although robust physical characteristics of rainfall changes can be found in the ALL and ANT multi-model means[15].

[1]Climate Research Division, Environment Canada, Toronto, Ontario M3H 5T4, Canada. [2]Nicholas School for the Environment and Earth Sciences, Box 90227, Duke University, Durham, North Carolina 27708, USA. [3]Department of Geography, 507 McCone Hall, University of California, Berkeley, California 94720, USA. [4]Climatic Research Unit, School of Environmental Sciences, University of East Anglia, Norwich NR4 7TJ, UK. [5]NOAA Earth System Research Laboratory, 325 Broadway, Boulder, Colorado 80305, USA. [6]Met Office Hadley Centre (Reading Unit), Meteorology Building, University of Reading, Reading RG6 6BB, UK. [7]National Institute for Environmental Studies, Tsukuba, Ibaraki 305-8506, Japan.

We estimated the combined effect of anthropogenic and natural external forcing on observed precipitation trends by regressing the observed trends onto the trends simulated in ALL simulations. Estimates of the individual influences of anthropogenic and natural forcing were similarly obtained by using the ANT and NAT4 simulation trend patterns respectively. The regression scaling factors that best match ALL and ANT simulation trends to the observed trends are shown in Fig. 3. The response to ALL, or to ANT alone, was detected in the observed trends in both periods; the response to natural forcing alone was not detected.

To separate the contributions from natural and anthropogenic forcing to observed trends, two-signal attribution analyses must be used[2,3]. Using combinations of two signal patterns from the ALL, ANT and NAT4 simulations in two-way regressions, we also found that the response to anthropogenic forcing is separable from the response to natural forcing and internal variability. The ANT and NAT responses were detected in the observed 50-year trends when ALL and ANT mean responses were used to estimate the contributions of ANT and NAT to trends (Fig. 3, right hand panel; see also Supplementary Fig. 7). The response to anthropogenic and natural forcings were also detected using the ALL4 and ANT4 ensembles

(Supplementary Fig. 7), indicating that the response to anthropogenic forcing can be reliably separated from the effects of natural forcing and internal variability, although the residual consistency test[25] failed in the latter case, indicating that internal variability might be underestimated, or that uncaptured aspects of the forced response have increased residual variability. This is consistent with an earlier study detecting volcanic influence on globally averaged land precipitation[10]. The estimated contribution of natural forcing to observed zonal precipitation trends is small in relation to the estimated contribution from anthropogenic forcing. From this and the separate detection of anthropogenic influence in a two-way analysis we conclude that the detected changes in observed land rainfall are largely in response to anthropogenic forcing.

A series of considerations show that the detection of an anthropogenic influence on precipitation is robust. While uncertainty in the magnitude of the observationally based estimate of precipitation change is considerable, there is little uncertainty in the sign of trend (see Supplementary Information). Thus sampling uncertainty is unlikely to have altered the observed pattern of latitudinal moistening and drying and is thus unlikely to nullify our detection results, which are based on the agreement in the observed and simulated
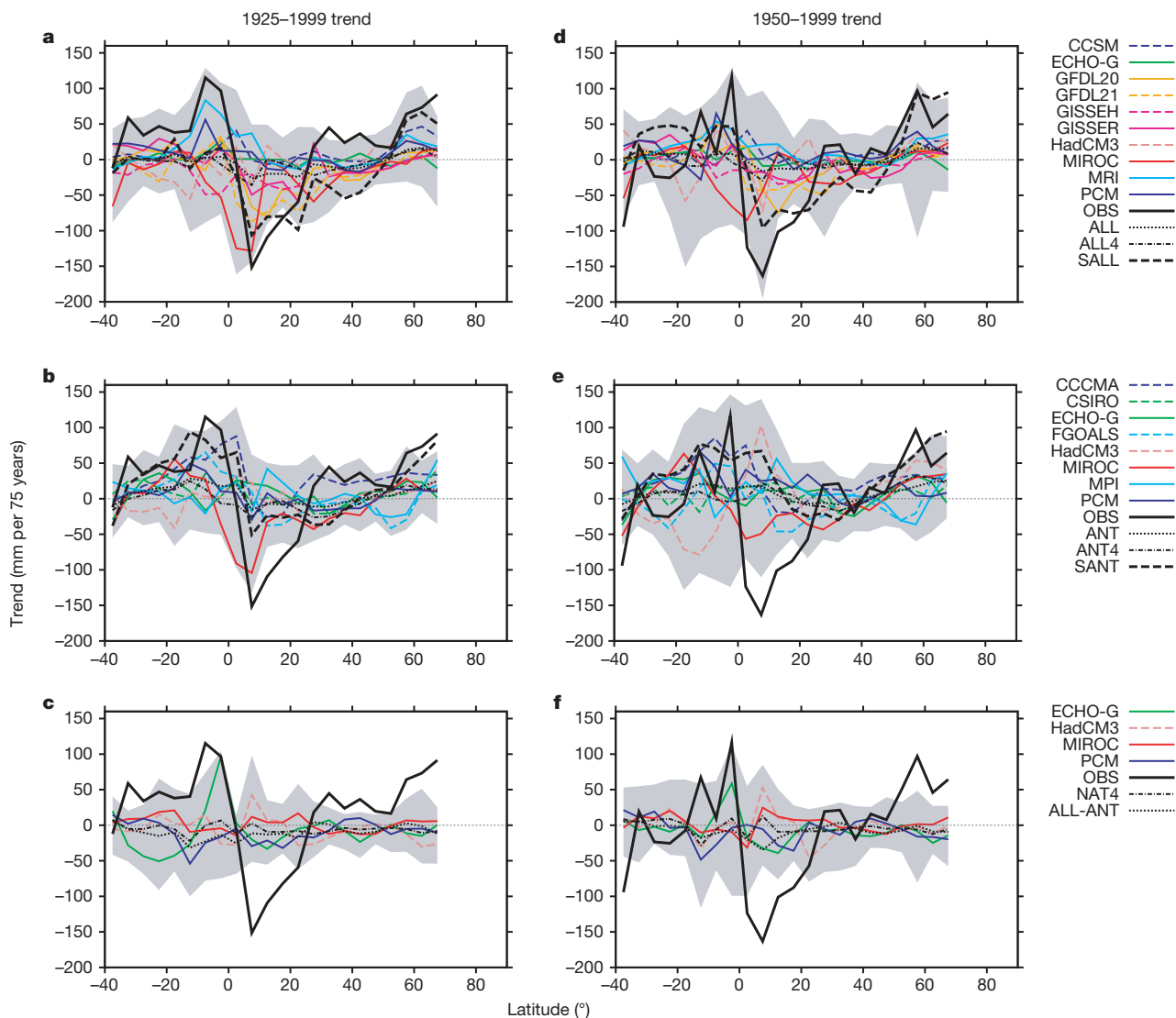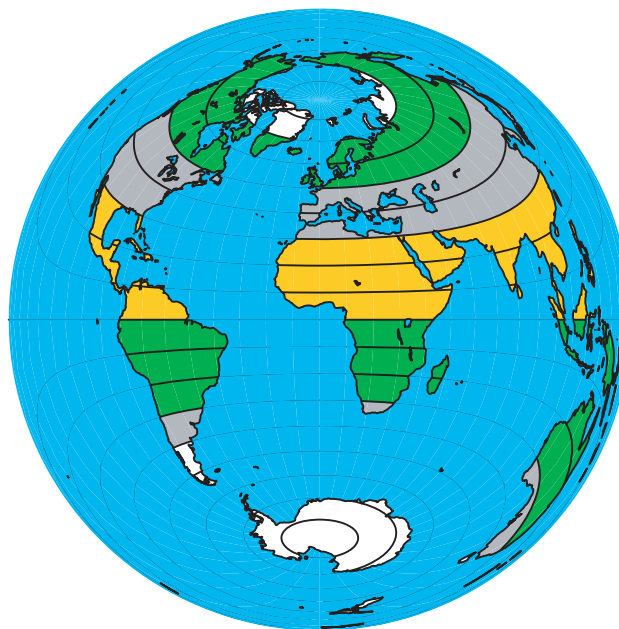

Figure 1 | Comparison between observed (solid black) and simulated zonal mean land precipitation trends for 1925–1999 (left) and 1950–1999 (right). Black dotted lines indicate the multi-model means from all available models (ALL in **a** and **d**, ANT in **b** and **e**, and NAT4 in **c** and **f**), and black dashed-dotted lines those from the subset of four models that simulated the response to each of the forcing scenarios (ALL4, ANT4 and NAT4). The model-simulated range of trends is shaded. Black dashed lines indicate ensemble means of ALL and ANT simulations that have been scaled (SALL and SANT) to best fit the observations based on a one-signal analysis. Coloured lines indicate individual model mean trends.
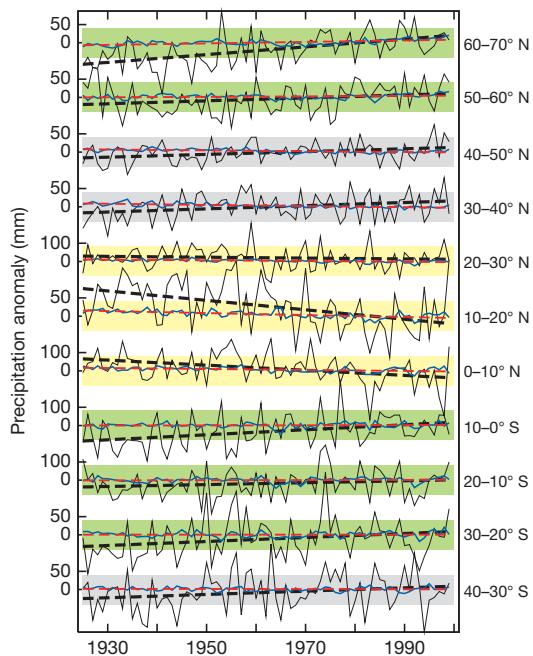
Figure 2 | 1925–1999 changes in observed and simulated precipitation anomalies. Time series (left panel) of observed annual zonal mean precipitation anomalies in 10° latitude bands (thin black trace) together with ensemble mean annual zonal mean precipitation anomalies in the 50 available ALL simulations (thin blue trace). Straight dashed black and red lines indicate the trends. Green (or yellow) shading identifies latitude bands with increasing (or decreasing) trends in both observations and models; grey shading indicates disagreement between observed and simulated trends. The map (right panel) indicates the different 10° latitude bands and whether trends agree in sign. Areas with insufficient data are shown in white. Only land precipitation data are used.

patterns of trends. Furthermore, our results are robust to the use of a data set that is based on less-complete observations and is gridded differently[22]. Our results are also robust to the use of signal patterns estimated from subsets of models, although, as expected, the robustness of detection deteriorates with decreasing number of models being used (not shown). Multi-model estimates of the pattern of external forcing response in precipitation are probably less susceptible to model error than are single model estimates[26]. The structure of the multi-model simulated fingerprint is consistent with our understanding of the mechanisms of precipitation response to anthropogenic forcing. It is expected that wet tropical regions would

become wetter and dry regions drier if there were an increase in tropospheric temperature from anthropogenic forcing but no change in lower-tropospheric relative humidity or flow[15]. The apparent shift in the Intertropical Convergence Zone is also consistent with hemispheric asymmetry in indirect aerosol forcing[20], although indirect aerosol forcing is not needed in all models to produce subtropical drying over land[15].

Because the observed record is relatively short and may be affected by the response to external forcing, we used climate models to estimate the variations in zonal rainfall trends expected from internal climate variability. This model-based internal variability estimate is
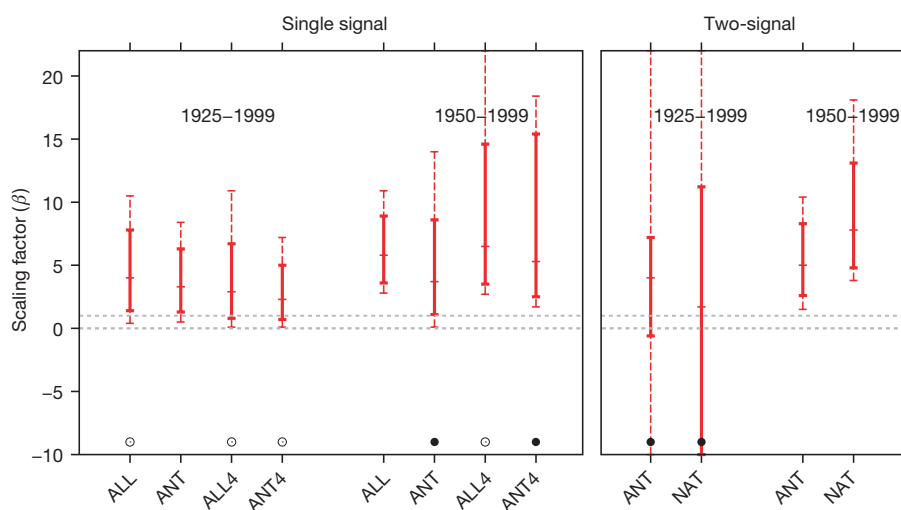
Figure 3 | Results from detection and attribution analysis of zonal precipitation anomalies. Scaling factors and their 5–95% uncertainty ranges are given from one-signal fingerprint detection analyses for ALL, ANT and NAT4 forced signals as well as subsets of four models, ALL4 and ANT4 (left panel) and from two-signal fingerprint detection analyses (right panel) for

ANT and NAT forced signals (see Fig. 1) The residual consistency test[25] passes except where indicated by open circles (test passes after doubling the estimate of internal variability) or closed circles (indicating that the test does not pass even after doubling). Dashed error bars correspond to 5–95% uncertainty ranges when the model simulated variance is doubled.

smaller than the observationally based estimate, particularly in the tropics, but a substantial part of the discrepancy may be the result of scale mismatch in the observational data (see Supplementary Information). Our finding of a detectable external influence on zonal precipitation trend holds when doubling the model-derived internal variance estimate, indicating that our finding is robust to possible moderate under-simulation of rainfall variability.

While the detection and attribution of an anthropogenic influence on zonal precipitation changes is robust, there are discrepancies in the magnitude of the changes. The multi-model mean significantly underestimates observed trends (Figs 1 and 3; see also ref. 27), consistent with the finding that the multi-model response to volcanic eruptions in global mean land rainfall is undersimulated[10]. The tropical mean precipitation responses simulated by atmospheric models to tropical ocean warming during El Niño events are also weaker than observed, despite correct simulation of the observed change in atmospheric column integrated water vapour[28,29]. A similar mechanism may be affecting tropical and subtropical zonal land rainfall changes here. Observational uncertainty might also have contributed to the discrepancy between observed and simulated trends. Furthermore, the statistical significance of the mismatch might be overestimated if the internal variability of precipitation is underestimated (Fig. 3). If the finding that observed changes are larger than simulated is robust, then projections may also underestimate future precipitation changes. However, some models in the ANT and ALL ensembles do show response features, particularly in the tropics, that are as large as those observed (see Fig. 1), but these are situated somewhat differently latitudinally, impeding detection and damping the amplitude of the multi-model pattern of response. Furthermore, different models contribute to different aspects of the multi-model mean response. Some models show little tropical response but increasing high-latitude precipitation, while others show a more realistic tropical and subtropical response but fail to increase high-latitude precipitation (see Fig. 1).

Overall, we find that anthropogenic forcing has had a detectable and attributable influence on the latitudinal pattern of large-scale precipitation change over the part of the twentieth century that we were able to analyse. Our best estimate of the response to anthropogenic forcing suggests (Fig. 1b) that anthropogenic forcing has contributed approximately 50–85% (5–95% uncertainty) of the observed 1925–1999 trend in land precipitation between 40° N and 70° N (62 mm per century), 20–40% of the observed drying trend in the northern subtropics and tropics (0° to 30°N; a decrease of 98 mm per century) and most (75–120%) of the moistening trend in the southern tropics and subtropics (0° to 30° S; 82 mm per century).

METHODS SUMMARY

Data processing. Observed annual land precipitation anomalies were obtained by subtracting the 1961–90 climatology from station monthly precipitation amounts[21] and summing monthly values if the year had at least 7 months with data. All other years were treated as missing. Annual values were gridded by averaging station values within $5° \times 5°$ latitude–longitude grid boxes. Zonal mean precipitation anomalies were obtained by averaging available annual anomalies within each latitudinal band.

Model data were first transferred to the same $5° \times 5°$ latitude–longitude grid as were the observations and subsequently processed in the same way as were the observations, including 'masking' missing values so that model values are available at the same times and places as the gridded observations.

Detection and attribution. The 'optimal fingerprint' method assumes that the observed trends $\mathbf{y}$ (organized as a vector with one entry per latitude band) may be represented as the sum $\mathbf{y} = \mathbf{X}\boldsymbol{\beta} + \mathbf{u}$ of scaled simulated responses to external forcing, or signals $\mathbf{X}$ (a matrix with one column for each signal considered) and natural internal variability $\mathbf{u}$. To account for uncertainty in the modelled response patterns, we used generalized total-least-squares[23] to estimate the scaling factors $\boldsymbol{\beta}$. Signals were estimated by averaging trends in all available model runs in the same forcing group. Two independent estimates of internal variability covariance, $\hat{\mathbf{C}}_{N1}$ and $\hat{\mathbf{C}}_{N2}$, which were needed for optimization and scaling factor estimation[2], were estimated from model simulations as in other studies[1–12].

We computed trends in 10° latitude bands to reduce the effects of internal variability. Our detection analysis is conducted in a subspace spanned by the first five leading empirical orthogonal functions of the estimated model covariance. The joint influences of ANT and NAT signals in observations were inferred from two-way regressions using combinations of two signal patterns from the multi-model ALL, ANT and NAT ensembles.

Full Methods and any associated references are available in the online version of the paper at www.nature.com/nature.

1. IDAG (International ad hoc Detection and Attribution Group). Detecting and attributing external influences on the climate system: A review of recent advances. *J. Clim.* **18**, 1291–1314 (2005).
2. Hegerl, G. C. *et al.* Multi-fingerprint detection and attribution of greenhouse-gas and aerosol-forced climate change. *Clim. Dyn.* **13**, 613–634 (1997).
3. Tett, S. F. B., Stott, P. A., Allen, M. R., Ingram, W. & Mitchell, J. Causes of twentieth-century temperature change near the Earth's surface. *Nature* **339**, 569–572 (1999).
4. Zhang, X., Zwiers, F. W. & Stott, P. A. Multi-model multi-signal climate change detection at regional scale. *J. Clim.* **19**, 4294–4307 (2006).
5. Stott, P. A. Attribution of regional-scale temperature changes to anthropogenic and natural causes. *Geophys. Res. Lett.* **30**, 1724, doi:10.1029/2003GL017324 (2003).
6. Gillett, N. P., Zwiers, F. W., Weaver, A. J. & Stott, P. A. Detection of human influence on sea level pressure. *Nature* **422**, 292–294 (2003).
7. Jones, G. S., Tett, S. F. B. & Stott, P. A. Causes of atmospheric temperature change 1960–2000: A combined attribution analysis. *Geophys. Res. Lett.* **30**, 1228, doi:10.1029/2002GL016377 (2003).
8. Santer, B. D. *et al.* Contributions of anthropogenic and natural forcing to recent tropopause height changes. *Science* **301**, 479–483 (2003).
9. Barnett, T. P. & Pierce, D. AchutaRao, K. Santer, B. & Gleicker, P. Penetration of human-induced warming into the world's oceans. *Science* **309**, 284–287 (2005).
10. Gillett, N. P., Weaver, A. J., Zwiers, F. W. & Wehner, M. F. Detection of volcanic influence on global precipitation. *Geophys. Res. Lett.* **31**, L12217, doi:10.1029/2004GL020044 (2004).
11. Lambert, F. H., Stott, P. A., Allen, M. R. & Palmer, M. A. Detection and attribution of changes in 20th century land precipitation. *Geophys. Res. Lett.* **31**, L10203, doi:10.1029/2004GL019545 (2004).
12. Lambert, F. H., Gillett, N. P., Stone, D. A. & Huntingford, C. Attribution studies of observed land precipitation changes with nine coupled models. *Geophys. Res. Lett.* **32**, L18704, doi:10.1029/2005GL023654 (2005).
13. Hulme, M., Osborne, T. J. & Johns, T. C. Precipitation sensitivity to global warming: comparison of observations with HadCM2 simulations. *Geophys. Res. Lett.* **25**, 3379–3382 (1998).
14. Dai, A., Fung, I. Y. & Del Genio, A. D. Surface observed global land precipitation variation during 1900–88. *J. Clim.* **10**, 2943–2962 (1997).
15. Held, I. M. & Soden, B. J. Robust responses of the hydrological cycle to global warming. *J. Clim.* **19**, 5686–5699 (2006).
16. Hegerl, G. C., Zwiers, F. W., Kharin, V. V. & Stott, P. A. Detectability of anthropogenic changes in temperature and precipitation extremes. *J. Clim.* **17**, 3683–3700 (2004).
17. Allen, M. R. & Ingram, W. J. Constraints on future changes in climate and the hydrologic cycle. *Nature* **429**, 224–232 (2002).
18. Cubasch, U. *et al.* in *Climate Change 2001: The Scientific Basis* (ed. Houghton, J. T. *et al.*) 525–582 (Cambridge Univ. Press, New York, 2001).
19. Emori, S. & Brown, S. J. Dynamic and thermodynamic changes in mean and extreme precipitation under changed climate. *Geophys. Res. Lett.* **32**, L17706, doi:10.1029/2005GL023272 (2005).
20. Rotstayn, L. D. & Lohmann, U. Tropical rainfall trends and the indirect aerosol effect. *J. Clim.* **15**, 2103–2116 (2002).
21. Vose, R. S. *et al. The Global Historical Climatology Network: Long-Term Monthly Temperature, Precipitation, Sea Level Pressure, and Station Pressure Data.* Report ORNL/CDIAC-53, NDP-041 (Carbon Dioxide Information Analysis Center, Oak Ridge National Laboratory, Oak Ridge, Tennessee, 1992); ⟨http://cdiac.esd.ornl.gov/ftp/ndp041/ndp041.pdf⟩.
22. Hulme, M. A. 1951–80 global land precipitation climatology for the evaluation of general circulation models. *Clim. Dyn.* **7**, 57–72 (1992).
23. Allen, M. R. & Stott, P. A. Estimating signal amplitudes in optimal fingerprinting. Part I: Theory. *Clim. Dyn.* **21**, 477–491 (2003).
24. Hasselmann, K. Multi-pattern fingerprint method for detection and attribution of climate change. *Clim. Dyn.* **13**, 601–612 (1997).
25. Allen, M. R. & Tett, S. F. B. Checking for model consistency in optimal fingerprinting. *Clim. Dyn.* **15**, 419–434 (1999).
26. Gillett, N. P. *et al.* Detecting anthropogenic influence with a multi-model ensemble. *Geophys. Res. Lett.* **29**, doi:10.1029/2002GL015836 (2002).
27. Wentz, F. J., Ricciardulli, L., Hilburn, K. & Mears, C. How much more rain will global warming bring? *Science* doi:10.1126/science.1140746 (2007); published online 31 May 2007.

28. Soden, B. J. The sensitivity of the tropical hydrological cycle to ENSO. *J. Clim.* **13**, 538–549 (2000).
29. Soden, B. J., Jackson, D. L., Ramaswamy, V., Schwarzkopf, M. D. & Huang, X. The radiative signature of upper tropospheric moistening. *Science* **310,** doi:10.1126/science.1115602 (2005).
30. Held, I. M., Delworth, T. D., Lu, J., Findell, K. L. & Knutson, T. R. Simulation of Sahel drought in the 20th and 21st centuries. *Proc. Natl Acad. Sci. USA* **102,** 17891–17896 (2005).

METHODS

Detection and attribution. Signals were obtained by averaging results from multi-model ensembles. This has been found to improve estimates of surface temperature response to anthropogenic forcing[4,26], suggesting that the bias in the multi-model mean is smaller than individual model biases[31].

The observed precipitation record is too short to provide estimates of $\hat{C}_{N1}$ and $\hat{C}_{N2}$ and may be affected by the response to external forcing. Internal climate variability is therefore estimated, as outlined below, from model simulations as in other studies[1–12]. More details are given in the Supplementary Information.

The covariance matrices were estimated from independent parts of a 1,700-year control simulation (which is divided into 17 non-overlapping 100-year samples) performed with model HadCM3, for which there is no year-to-year change in external forcing, and from variability between members in ensembles of forced simulations. The latter consist of a total of 9,200 years of climate simulation with ALL, ANT or NAT forcing in ensembles of three to nine 100-year simulations (Supplementary Table 1).

For the 75-year detection analysis, trends were estimated from the last 75 years of the 100-year samples of model output that were masked to mimic the availability of gridded observations during 1925–99. For the 50-year detection analysis, we split each of the 100-year chunks of data into two 50-year periods, and computed trends in each 50-year data segment that was masked to mimic the 1950–1999 availability of gridded observations. We then partitioned the control and forced simulations in such a way that every model is represented in the covariance matrix estimates $\hat{C}_{N1}$ and $\hat{C}_{N2}$. In the case of ensembles with an odd number of members k, we assigned $(k + 1)/2$ members randomly to either sample N1 or N2, and the remaining members were allocated to the other sample; the allocation of the larger number of members was alternated between models to ensure that N1 and N2 contain the same number of members in total. In the case of ensembles with an even number of members, half of the members were randomly allocated to each sample. Overall mean trend patterns were removed separately from the control, ALL, ANT and NAT simulations in each sample N1 and N2, and the residual trends were used to estimate C_{N1} and C_{N2}. The covariance estimates were appropriately adjusted to reflect the fact that ensemble mean trend patterns were removed from individual ensembles.

Because model data for estimating the covariance matrix were limited, and because optimal detection involves inversion of the estimated covariance matrix[23,24], we had to conduct our detection analysis in a reduced dimension space. This was accomplished by first calculating trends in 10° latitude bands to reduce the effects of internal variability. The spatial pattern of trends at this coarser resolution preserves most of the structure seen in 5° bands. Dimensionality was further reduced by retaining only the first five leading empirical orthogonal functions of the estimated model covariance. Model-based and observation-based estimates of precipitation variability are more often consistent with each other in this reduced dimension space according to a standard test[25], indicating that this space retains only the more robustly simulated aspects of rainfall change, and that the covariance matrix is robustly estimated. This truncation preserves the spatial pattern of trends, including key physical aspects, and retains more than 76% of signal variance (see Supplementary Information). It is of concern that model simulated precipitation variability is generally lower than observationally based estimates. However, the latter are probably biased high owing to sampling noise in the observations (see Supplementary Information).

The optimal detection method described previously was used to determine whether the responses to ALL, ANT and NAT signals are individually detectable in observed trends in zonal mean precipitation. However, two-signal attribution analyses must be used to separate the contribution from natural and anthropogenic forcing to observed trends. Thus the joint influence of ANT and NAT signals in observations was inferred from two-way regressions using combinations of two signal patterns from the multi-model ALL, ANT and NAT4 ensembles. Relatively few NAT only simulations were available for our analysis, so the most robust two-signal analysis results were obtained using the ALL and ANT ensembles; the contribution from ANT and NAT separately could be derived from a linear combination of the scaling factors of ALL and ANT[2]. Scaling factors estimated jointly in two-signal detection analysis were generally correlated (see Supplementary Information).

The methods used to make inferences about the scaling factors $\boldsymbol{\beta}$ and the residual consistency assume that the natural internal variability $\mathbf{u}$ is gaussian-distributed. While daily precipitation is far from gaussian, the Central Limit Theorem indicates that the large-area averages of annual mean precipitation anomalies that are used in our analysis should nevertheless be approximately gaussian. Repeating our analyses using transformed annual anomalies assuming a gamma distribution for the annual anomalies produced very similar detection and attribution results.

31. Kharin, V. V., Zwiers, F. W. & Zhang, X. Intercomparison of near-surface temperature and precipitation extremes in AMIP2 simulations, reanalyses, and observations. *J. Clim.* **18**, 5201–5223 (2005).

Author Queries

Query Reference	Query
1	AUTHOR: When you receive the PDF proofs, please check that the display items are as follows (doi:10.1038/nature06025): Figs 1, 2, 3 (colour); Tables: None; Boxes: None. Please check all figures very carefully as they have been re-labelled, re-sized and adjusted to Nature's style. Adjectives derived from proper nouns (such as gaussian) are lower-cased. Please ensure that any error bars in the figures are defined in the figure legends.
2	Author: colour of thin red line changed to blue to make it more visible,OK?

For Nature office use only:

Layout	☐	Figures/Tables/Boxes	☐	References	☐
DOI	☐	Error bars	☐	Supp info (if applicable)	☐
Title	☐	Colour	☐	Acknowledgements	☐
Authors	☐	Text	☐	Author contribs (if applicable)	☐
Addresses	☐	Methods (if applicable)	☐	COI	☐
First para	☐	Received/Accepted	☐	Correspondence	☐
Display items	☐	AOP (if applicable)	☐	Author corrx	☐